Log wavelet Leaders cumulant based multifractal analysis of EVI fMRI time series: evidence of scaling in ongoing and evoked brain activity

Philippe Ciuciu *Member, IEEE*, Patrice Abry, *Senior Member, IEEE*, Cécile Rabrait and Herwig Wendt

***Abstract*— Classical within-subject analysis in functional Magnetic Resonance Imaging (fMRI) relies on a detection step to localize which parts of the brain are activated by a given stimulus type. This is usually achieved using model-based approaches. Here, we propose an alternative exploratory analysis. The originality of this contribution is twofold. First, we propose a synthetic, consistent and comparative overview of the various stochastic processes and estimation procedures used to model and analyse scale invariance. Notably, it is explained how multifractal models are more versatile to adjust the scaling properties of fMRI data but require more elaborated analysis procedures. Second, we bring evidence of the existence of actual scaling in fMRI time series that are clearly disentangled from putative superimposed non stationarities. By nature, scaling analysis requires the use of long enough signals with high frequency sampling rate. To this end, we make use of a Localized 3D Echo Volume Imaging (EVI) technique, which has recently emerged in fMRI because it allows very fast acquisitions of successive brain volumes. High temporal resolution EVI fMRI data have been acquired both in resting state and during a slow event-related visual paradigm. A voxel-based systematic multifractal analysis has been performed over both kinds of data. Combining multifractal attribute estimates together with paired statistical tests, we observe significant scaling parameter changes between ongoing and evoked brain activity, which clearly validate an increase in long memory and suggest a global multifractality decrease effect under activation.**

***Index Terms*— Biomedical signal detection, functional Magnetic resonance imaging, Multifractal analysis, Wavelet Leaders, brain activity, EVI.**

I. Motivation: scaling in fMRI?

While classical data analysis procedures in functional Magnetic Resonance Imaging (fMRI) rely on a model of the expected BOLD (Blood oxygen Level Dependent) response for localizing evoked activity *i.e.,* specific brain regions involved in the performance of cognitive or behavioral tasks, exploratory analysis aims at finding significant components in the data that explain most of the fluctuations in a model-free manner. A post-hoc classification of these components is often used to discriminate physiological trends related for instance to cardiac beat or breathing rate from stimulus-induced (i.e. evoked) activity. In most cases, one is interested in extracting spatial components using multivariate methods like Principal or Independent Components Analysis techniques [1–3]. In the present work, we rather concentrate on a univariate *model-free framework* which is able to clearly disentangle true scaling behaviors from non-stationary trends superimposed to the BOLD signal irrespective of the presence of an external stimulation (resting state or evoked activity).

The presence of scale invariance in fMRI data has been considered as confound or noise for a long time. Indeed, fMRI time series are known to have a colored noise structure, the majority of which occurs at low frequency. Preliminary evidence that fMRI time series have long memory in time or $1/f$ spectral properties has been demonstrated on "resting state" motion-corrected datasets [4, 5]. Previous studies have shown that head movement is a common source of long memory noise caused by slow rotation or translation of the subject's head through an imperfectly homogeneous magnetic field [6, 7]. Physiological factors such as cardiac beat or breathing cycle may also contribute to this scaling phenomenon since they may contaminate the BOLD signal with properties depending on the sampling period of data (*i.e.,* short/long time of repetition (TR)) [8–10]. Early investigations therefore considered these space-varying low frequency components as noise, which are responsible for potential non stationarities [11–13]. Hence, to fulfill the assumptions underlying the classical model-based localization techniques of brain activity, most neuropsychologists resort to high-pass filtering to remove these trends. In the last few years, the Generalized Linear Model estimation method has been extended to account for $1/f$ (or fractional Gaussian) noise using wavelet decomposition [14]. More recently, it has been demonstrated that a Bayesian approach incorporating nonstationary noise models outperforms the classical GLM-based techniques in terms of activation detection [15]. The latter actually loses crucial dynamic features in the data.

Other authors have pointed out that the BOLD signal itself contains power at virtually all frequencies, notably in randomized event-related designs [16]. Interestingly, recent studies have reported that low-frequency spatial fluctuations in cortical BOLD signals may be indicative of synchronized long memory neuronal oscillations rather than merely noise [17–19]. Concomitantly, greater persistence during brain activation has been found in normal subjects in [18]. This confirms that high-pass filtering may potentially remove parts of the signal of interest. Also, higher predictability summarized in terms of scaling exponent (controlling the power law decrease of $1/f$ spectra) has been reported in patients with Alzheimer disease

Philippe Ciuciu and Cécile Rabrait are with CEA/NeuroSpin, Gif-sur-Yvette, France. Phone/Fax: 33 16908 7785/7980. E-mails: firstname.lastname@cea.fr.

Patrice Abry and herwig Wendt are with Physics Lab., CNRS UMR 5672, Ecole Normale Supérieure de Lyon, France. Phone/Fax: 33 47272 8493/8080. E-mails:firstname.lastname@ens-lyon.fr.

Submission dates: 03/15/2008

or with major depressive disorder, especially in brain regions implicated in the early stages of the degeneracy process [19, 20].

Inspired by the connection between $1/f$ and long range dependence, several groups have argued that the analysis of fMRI time series should be performed in the wavelet domain [5, 12, 14, 15, 19]. Then, a first attempt to identify stimulus-induced signal changes from scaling parameters has been proposed in [18, 21]. These authors have developed voxel-based fluctuation analysis (FA), compared it to wavelet multiresolution analyses (*e.g.,* the wavelet transform modulus maxima method [22, 23]), and applied it to high temporal resolution fMRI data. Interestingly, they have shown that the fractal feature of voxel time series can be utilized to separate active and inactive brain regions [18, 21]. Also, to decide whether scaling analysis can help distinguish motion artifacts from true BOLD responses, complementary analyses have been conducted in [24]. They are based on detrended fluctuation analysis (DFA) and conclude that DFA succeeds in distinguishing among three types of voxels, noise, motion artifacts, and true BOLD responses when classical FA fails to robustly recognize which active regions in the brain are truly involved in certain tasks. However, it has been argued in [25] that wavelet tools perform better than DFA. Therefore, in the present contribution, the voxel-based analysis of scaling properties is based on wavelet decompositions. To enrich the description of scaling properties of data, the model of $1/f$ processes has been associated to that of long range dependence. These classes of models have then been embodied into that of self-similar processes. Further, multifractal processes were proposed has another versatile class of models for scale invariance. All these notions are often confusingly taken one for the other.

Therefore, the first goal and contribution of the present article is of tutorial nature. It is intended to give a brief yet precise and tutorial introduction to the concepts, stochastic models and analysis tools tied to scale invariance. Scale invariance can be fruitfully described with a nested suite of stochastic models, (2nd order stationary) $1/f$-processes, self-similar processes and multifractal processes. This collection of models possesses an increased versatility (mostly a larger number of parameters) to capture the richness of scaling properties in data; at the price, though, of substantially increased difficulties both in their definitions and analysis methodologies. The use of self-similar processes provides the practitioners with a better mathematically grounded framework to perform scaling exponent estimation of data. The use of multifractality rather than self-similarity to model data implies two major conceptual changes: i) the single scaling parameter defining self-similar processes is replaced with a collection (multi-fractal) of scaling parameters, ii) scaling analysis can no longer be based on classical multiresolution quantities, such as increments or (discrete or continuous) wavelet coefficients [26], and should rather rely on new multiresolution quantities bringing significant robustness and gains in estimation performance: the *wavelet Leaders* [27]. Also, instead of the classical *structure function* based procedures [26, 28], MF attributes are estimated from the logarithm of the wavelet Leaders. These theoretical elements are introduced in Section II whose aim and originality consist of guiding the reader, in a self-consistent and homogeneous manner, through the declinations of the refined stochastic models that can be used to describe scaling as well as through the necessary adaptation of the analysis tool. The second goal and contribution of the present article consists of applying scaling analyses to high temporal resolution BOLD fMRI data acquired during a 3D parallel localized Echo Volumar Imaging (EVI) sequence [29] (cf. Section III). As opposed to conventional EPI, this new imaging technique makes multi-slice acquisition in a few hundreds of milliseconds feasible. Our goal is therefore to analyze whether such data collected during resting state and under a slow event-related visual protocol do possess scaling or not and what their nature is (self-similarity or multifractal). Results are reported in Section IV-A. It is shown that this *log-cumulant* wavelet-Leader based approach enables us to bring evidence for the existence of scaling in fMRI time series for both kinds of data and to characterize their nature. Also, we illustrate that such scaling cannot be confused with putative non stationary trends superimposed to data. A set of statistical tests enable us to conclude that activation induces a clear and systematic increase of the long memory parameter with a (less strong and systematic) decrease in multifractality. This is discussed in Section V.

II. Scaling and multifractal: theory

A. Scale invariance (or scaling)

Classically, data analysis often amounts to trying to identify one (or a few) particular scale(s) of time that play(s) a specific role in the data dynamics and to basing data description on models whose key parameters are controlled by these specific time-scale(s). Scale invariance consists of the negation of this approach: No scale of time (or space) can be singled out or found as having a characteristic importance. It can also be reformulated as the fact that all the scales are equally contributing to data dynamics. Scale invariance has primarily been connected to (2nd order stationary) $1/f$-processes and to spectrum estimation. Let X denote the signal under analysis, and $\hat{\Gamma}_X(f, t_k)$ any standard spectrum estimation procedure, such as Welch estimator or such as average over sliding time windows (centered around times t_k) of the squared smoothed Fourier transforms (periodograms): Scale invariance is then associated to a power law behavior of the spectrum estimate with respect to a wide range of frequencies, $f \in [f_m, f_M], f_M/f_m \gg 1$:

$$\frac{1}{n}\sum_{k=1}^{n} \hat{\Gamma}_X(f, t_k) \simeq C|f|^{-\gamma},\ \gamma > 0. \qquad (1)$$

However, it is now well established (e.g., [28, 30]) that $1/f$-processes and standard spectral estimation have limited capacities both for modeling and analyzing scaling. For instance, the power law behavior of the spectrum cannot simultaneously hold in both limits ($|f| \to 0$ and $|f| \to +\infty$) and a $1/f$ spectrum constitutes only a rough definition for a class of models. Along the same line, standard spectral analysis tools provide the practitioners with poor estimates of the scaling exponent

γ. Such tools also turn out to encounter severe limitations in enabling to distinguish between true power law spectral behavior and low frequency (or slow) non stationarities, trends or drifts that may also exist in data. More specifically, in the context of fMRI, low frequency drifts have been measured in phantoms and cadavers [31]. It has also been observed that high frequency physiological components can be aliased in low frequencies. Therefore, it has often been thought that the scaling properties that are observed in data actually only correspond to artifacts caused by non stationary behaviors. This motivated a first major change: Standard spectral estimates $\hat{\Gamma}_X(f,t_k)$ are replaced with multiresolution quantities, labeled $T_X(a,t)$, i.e., quantities describing the content of X around a time position t, and a scale a. Qualitatively, the analysis scale a acts as the inverse of a frequency: $a \sim f_0/f$ (f_0 being a constant that depends on the details of the definition of $T_X(a,t)$). Standard examples for $T_X(a,t)$ are given by wavelet, increment or box-aggregated coefficients. Moreover, wavelet transforms have been shown to provide practitioners with relevant analysis of scaling properties, notably in terms of robustness against non stationarity (see e.g. [28, 30, 32–35]). Another significant change in scaling modeling lies in the fact that one now commonly considers not only second order statistical analysis but instead a collection of statistical orders q [28]. Therefore, scale invariance is now commonly and operationally defined as the power law behaviors of the (time average of the $q-$th power of the) $T_X(a,t)$, with respect to the analysis scale a, for a given (large) range of scales $a \in [a_m, a_M], a_M/a_m \gg 1$:

$$\frac{1}{n_a}\sum_{k=1}^{n_a} |T_X(a,k)|^q \simeq c_q a^{\zeta(q)}. \tag{2}$$

The $\zeta(q)$ are referred to as the scaling exponents and their estimation is often the major goal in scaling analysis. The estimated exponents are often used for data identification or classification. In the present application to fMRI data, the goal is to investigate whether the values of the scaling exponents are varied under brain activity stimulation.

This new definition is made consistent by the use of new stochastic processes to fruitfully model scale invariance: self-similar processes [36] and multifractal processes [37]. They are introduced in the remainder of this section together with the details of the corresponding wavelet based analyses.

B. Multiresolution quantities

1) Wavelet coefficients: Let $\psi_0(t)$ denote the *mother-wavelet*: an elementary function, characterized by a fast exponential decay and a strictly positive integer $N \geq 1$, the *number of vanishing moments*, defined as $\forall k = 0, 1, \ldots, N-1$, $\int_{\mathcal{R}} t^k \psi_0(t) dt \equiv 0$ and $\int_{\mathcal{R}} t^N \psi_0(t) dt \neq 0$. The mother-wavelet is moreover chosen such that the collection of templates of ψ_0 dilated to scales 2^j and translated to time positions $2^j k$, $\{\psi_{j,k}(t) = 2^{-j}\psi_0(2^{-j}t - k), j \in \mathcal{Z}, k \in \mathcal{Z}\}$, forms an orthonormal basis of $L^2(\mathcal{R})$. The discrete wavelet transform (DWT) of X is defined through its coefficients:

$$d_X(j,k) = \int_{\mathcal{R}} X(t)\, 2^{-j}\psi_0(2^{-j}t - k)\, dt. \tag{3}$$

Note the choice of the L^1-norm (as opposed to the more common L^2-norm choice) that better matches scaling analysis. For further details on wavelet transforms, the reader is referred to e.g., [38].

2) Structure functions: For fixed scales $a = 2^j$, the time averages of (the q-th powers of) the $d_X(j,k)$ are referred to as the structure functions (with n_j the number of $d_X(j,k)$ available at scale 2^j).

$$S^d(j,q) = \frac{1}{n_j}\sum_{k=1}^{n_j} |d_X(j,k)|^q. \tag{4}$$

3) Wavelet Leaders: Let us further assume that $\psi_0(t)$ has compact time support and define dyadic intervals as $\lambda \equiv \lambda_{j,k} = \left[k2^j, (k+1)2^j\right)$. Also, let Λ denote the union of the interval λ with its 2 adjacent dyadic intervals: $\Lambda \equiv \Lambda_{j,k} = \lambda_{j,k-1} \cup \lambda_{j,k} \cup \lambda_{j,k+1}$. Following [27, 39], we define the wavelet Leaders as (Fig. 1 illustrates this definition) :

$$L_X(j,k) \equiv L_\lambda = \sup_{\lambda' \subset \Lambda_{j,k}} |d_{\lambda'}|. \tag{5}$$

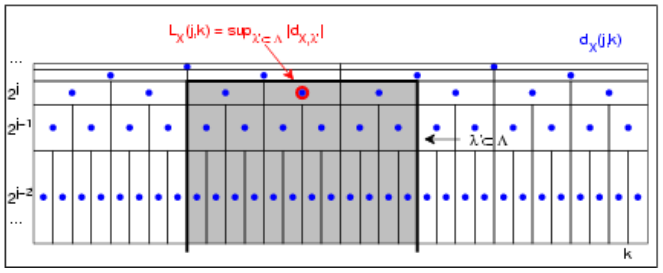

Fig. 1. **Definition of Wavelet leaders.** The wavelet Leader $L_X(j,k)$, located on node $(k2^j, 2^j)$ (red circle) of the dyadic grid underlying the DWT, is (practically) obtained as the largest of all wavelet coefficients $d_X(j',k')$ located at finer scales $j' \leq j$ within in a time neighborhood $(k-1)2^j \leq k'2^{j'} < (k+2)2^j$ (blue dots within the grey-shaded area).

C. Scaling models: Long range dependence, Self-similarity, Multifractality

1) Long range dependence (LRD): As mentioned in Section I, the oldest intuition associated to scaling or scale invariance traces back to $1/f$-processes, i.e., to (second-order) stationary processes Y whose spectrum behaves, for some (wide) range of frequencies, as,

$$\Gamma_Y(f) \simeq C|f|^{-\gamma} \tag{6}$$

with $\gamma > 0$. In the particular case where the power law behavior holds in the limit $f \to 0$ and for $0 \leq \gamma \leq 1$, the process Y is said to be long range dependent or to possess long memory [36]. The wavelet coefficients $d_Y(j,k)$ of Y are related to its spectrum via

$$2^j \mathbb{E}|d_Y(j,k)|^2 = \int_{\mathcal{R}} \Gamma_Y(f)|\Psi_0(2^j f)|^2 df, \tag{7}$$

where Ψ_0 denotes the Fourier transform of ψ_0 [28]. For LRD processes, it implies the following asymptotic power law behavior of the (power of the) wavelet coefficients:

$$2^j \mathbb{E}|d_Y(j,k)|^2 = 2^j \mathbb{E}S_Y(j,2) \sim C_\psi 2^{j\gamma-1},\ 2^j \to +\infty. \tag{8}$$

2) Self-similarity (SS): Long range dependence involves only the description of the statistical second-order ($q = 2$) of data. Self-similar processes provide us with a better mathematically grounded framework to model scale invariance. A process X is said to be self-similar when it satisfies $\forall c > 0, \{X(t), t \in \mathcal{R}\} \overset{fdd}{=} \{c^H X(t/c), t \in \mathcal{R}\}$, where $\overset{fdd}{=}$ means equality of all finite dimensional distributions [36]. For finite variance and stationary increment self-similar processes (of interest here and denoted $H-$sssi), the self-similarity parameter H is restricted to $H \in (0, 1)$, and one can show that [28, 40]:

$$S^d(j, q) = C_q 2^{jqH}, \forall\, 2^j, q \in (-1, +\infty). \tag{9}$$

When $1/2 < H < 1$, the increments Y of X are LRD, with $\gamma = 2H - 1$. This is why SS and LRD properties are often confused one with the other. Note, however, that Y is stationary when X is not and that LRD involves only the second statistical order and the limit of coarse scales ($a = 2^j \to +\infty$) when SS involves all statistical orders and all scales, from finest to coarsest ($0 < a = 2^j < +\infty$).

Self-similarity consists of a demanding model with respect to empirical data as it requires, first, that the scaling property holds for all scales and second, that the single parameter H controls all the statistical properties of the data. From a practical perspective, this is often too severe a limitation and multifractal models are preferred.

3) Multifractality: Multifractal (MF) processes are often considered as a further extension to model scale invariance since they enable to account for a declination of scaling properties often observed on empirical data: For a range of orders q and a range of scales 2^j, the structure functions of MF processes exhibit power law behaviors with respect to (wrt) scales, for a given range of scales, (cf. [28, 40]),

$$S^d(j, q) = C_q^d 2^{j\zeta(q)},\ q \in [0, q_*^+], \tag{10}$$

where the scaling exponent $\zeta(q)$ have a concave shape that hence depart from the linear behavior qH, seen as the signature of self-similarity (cf. Eq. (9)). This amounts to reading $\zeta(q)$ as a collection of scaling exponents replacing the single self-similarity parameter H and, hence, bringing versatility in actual data modeling.

A detailed introduction to multifractal theory is beyond the scope of this contribution, the reader is referred to e.g., [27, 37, 40]. We only restate here a few key points. Concave scaling exponents imply that the scales involved in the scaling of Eq. (10) necessarily has an upper bound, hence that scaling hold at fine scales only. Multifractal analysis is often theoretically phrased in terms of the multifractal spectrum $D(h)$ rather than in terms of scaling exponents $\zeta(q)$. This function $D(h)$ is theoretically designed to convey the scaling properties in terms of locally singular behaviors. For a number of (commonly used) stochastic processes and for all applied purposes, these two functions are related one to the other by a Legendre transform and hence strictly equivalent:

$$D(h) = \inf_{q \neq 0} \left(1 + qh - \zeta(q)\right). \tag{11}$$

Multifractal theory indicates that the measurement of the entire function $D(h)$ requires the use of both positive and negative values of q and hence that a practically relevant multifractal analysis of data should extend Eq. (10) above to negative q.

Obviously, wavelet coefficients, because they mostly take values close to 0, cannot be raised to negative powers and the corresponding structure functions $S^d(j, q)$ turn unstable. Also, even when using positive q, it has been shown [39, 40] that the use of $S^d(j, q)$ can only poorly enable the practical discrimination between a linear behavior qH and a concave $\zeta(q)$, hence do not permit to accurately distinguish between self-similar and multifractal processes. To overcome this drawback, the use of wavelet Leaders (as defined above) instead of wavelet coefficients has been proposed and shown to be both theoretically and practically (estimation performance) more accurate. This amounts to rewriting Eq. (10) above as,

$$S^L(j, q) = C_q^L 2^{j\zeta(q)},\ \text{for a range of } 2^j,\ q \in [q_*^-, q_*^+]. \tag{12}$$

This is referred to as the Wavelet Leader Multifractal formalism (WLMF). For self-similar processes, the equation above reduces to $S^L(j, q) = C_q^L 2^{jqH}$, $\forall q \in \mathcal{R}$.

D. Empirical scaling (or multifractal) analysis

1) Log-Cumulant: Measuring the function $\zeta(q)$ from data theoretically implies to perform estimation for all q. Instead, it has been suggested [26, 41] to envisage polynomial expansion of $\zeta(q)$:

$$\zeta(q) = \sum_{p=1}^{\infty} c_p^L \frac{q^p}{p!}. \tag{13}$$

It can be shown [26, 39, 41] that the coefficients c_p^L can be obtained from the scale dependence of $C^L(j, p)$, the cumulant of order $p \geq 1$ of the random variable $\ln |L_X(j, \cdot)|$:

$$\forall p \geqslant 1, C^L(j, p) = c_{0,p}^L + c_p^L \ln 2^j \tag{14}$$

Therefore, the knowledge of $\zeta(q)$ and hence of $D(h)$ can be recast into that of the *log-cumulants* c_p^L. This is of practical interest as self-similar processes are characterized by $\forall p \geq 2 : c_p^L \equiv 0$ (or $c_p^d \equiv 0$), while for multifractal processes of interest $c_2^L \neq 0$ (or $c_2^d \neq 0$). For the multifractal case, when time series are short as in fMRI, c_1^L and c_2^L gather most of the information practically available from $D(h)$ or $\zeta(q)$: c_1^L characterizes the location of the maximum of $D(h)$, while c_2^L is related to its width. In the systematic analysis of the voxels reported below, we will therefore concentrate on such two parameters and thus on parabolic approximations of the multifractal characterizations: $\zeta(q) \simeq c_1^L q + c_2^L q^2/2$ and $D(h) \simeq 1 - (h - c_1^L)^2/(2c_2^L)$.

2) Estimation procedures: Practical scaling analysis or empirical MF analysis mostly amounts to measuring the *scaling exponents* $\zeta(q)$, or equivalently the *log-cumulants* c_p, from the observed data. This is performed by tracking straight lines and estimating slopes in log-log plots (often referred to as logscale diagrams), as suggested by Eqs. (12) or (14) above.

From n_j wavelet coefficients $d_X(j,k)$, wavelet Leaders are computed (according to Eq. (5)). Then, standard estimation procedures are used to obtain the estimates $S^L(j,q)$ and $\hat{C}^L(j,p)$. From these, the corresponding $\hat{\zeta}^L(q)$ and c_p^L can then be estimated by linear regression (*cf.* Eq. (14)),

$$\hat{\zeta}^L(q) = \sum_{j=j_1}^{j_2} w_j \log_2 S^L(j,q), \tag{15}$$

$$\hat{c}_p^L = \log_2 e \sum_{j=j_1}^{j_2} w_j \hat{C}^L(j,p). \tag{16}$$

The weights w_j have to satisfy the constraints $\sum_{j_1}^{j_2} j w_j \equiv 1$ and $\sum_{j_1}^{j_2} w_j \equiv 0$ and can be expressed as $w_j = b_j^{-1} \frac{V_0 j - S_1}{V_0 V_2 - V_1^2}$ with $V_i = \sum_{j_1}^{j_2} j^i b_j^{-1}$, $i = 0:2$. As in [28], we chose $b_j = n_j^{-1}$ to perform weighted linear fits.

3) Other scaling analysis procedures: The estimation procedures can be rewritten directly using the (absolute value of the) wavelet coefficients $|d_X(j,k)|$ instead of the Leaders $L_X(j,k)$, yielding mutatis mutandis the estimates $\hat{\zeta}^d(q)$, $\hat{c}_p^d$. This is referred to as the Wavelet Coefficient Multifractal formalism (WCMF). Until a recent past, this WCMF was the only MF formalism available. However, it has recently been established that Leaders enable to measure the entire multifractal spectrum (through the use of negative q) [27, 40] and present far better performance [39, 42] as soon as one tries to discriminate between linear and concave $\zeta(q)$ functions.

An earlier solution to the negative q issue had been proposed (see *e.g.,* [26]). It is based on the Modulus Maxima of the CWT. However, wavelet Leaders provide us with a better mathematically grounded solution, exhibit a far lower computational cost, and can be readily extended to processes of higher dimensions (to images for instance).

4) Illustration: An example of the resulting estimations for $\zeta(q)$ and $D(h)$ (detailed below) is reported in Fig. 7 for a representative voxel in the visual cortex eliciting activation.

To finish with, let us mention that multifractal analysis can be applied to any kind of data or processes, be they multifractal or not, just as Fourier analysis can be applied to any signal be they pure harmonic tones or not.

III. Data acquisition

A. Why do we use EVI fMRI datasets?

Irrespective of the retained approach, analysis of scaling behavior implies long enough signals. In [21], the authors tested their MF analysis on Echo Planar Imaging (EPI) fMRI data, which temporal resolution was decreased down to 200ms for partial brain volume acquisition to get up to 1500 time points. Here, we resort to a new imaging technique called parallel localized EVI, recently validated on the human brain [29]. This imaging procedure offers a very high temporal resolution (one volume every 200ms) and thus enables acquisition of a larger number of brain volumes (not only a single slice) in a standard acquisition period (here 2210 scans). This offers the possibility to perform reliable scaling analyses. The present study therefore aims at exploring the benefit of this new leader based MF analysis in combination with EVI brain images, which are highly resolved in time, as described in the next part.

B. Echo-Volumar Imaging technique

The principle of EVI has been introduced in [43]. Faster than EPI, EVI allows 3D single-shot acquisition at very high scanning rates. Nevertheless, this acquisition technique requires very high performances from the MR hardware in order to avoid signal losses and geometric distortions due to B_0 inhomogeneities and long echo train durations. Thus, only a few attempts at using EVI in fMRI have been performed until now, focusing mainly on very anisotropic brain volumes [44, 45]. Due to improved gradient hardware and magnet homogeneity, and especially to the application of parallel acquisition and reconstruction, we demonstrated the feasibility of acquiring large, isotropic, brain volumes with EVI, at usual fMRI spatial resolution, in about 200 ms [29]. Localized Parallel EVI relies on the use of outer volume suppression pulses and parallel acquisition with undersampling by a factor of 2 along two directions, in order to reduce the echo train durations by a factor of 4, as described in Fig. 2. Consequently, a $120 \times 120 \times 144\text{mm}^3$ brain volume can be acquired in 200 ms, with a distortion level comparable to EPI. Parallel reconstruction was performed using an in-house-developed multidimensional SENSE algorithm, which requires one sensitivity map for each acquisition channel. In order to improve signal stability in the reconstructed time series, parallel reconstruction was regularized, as pioneered in [46, 47]. Tikhonov weighting was applied, with a regularization condition minimizing the magnitude of the MR signal in the reconstructed volumes, as proposed in [48]. The relative importance of the regularization term was modulated by a regularization parameter λ^2, empirically set.

All experiments were performed on a 1,5 T GEHC scanner (40 mT/m, 150T/m/s slew rate gradient, 8 channel head coil array). EVI acquisitions have been performed using the following parameters: orientation= sagittal plane, TE/TR $= 40/200$ ms, flip angle (FA) $= 35°$, BW $= 62.5$ kHz, FOV $= 80 \times 80 \times 100$ mm^3, acquired/reconstructed matrices $= 20 \times 10 \times 10/20 \times 20 \times 20$, echo train duration = 60.5 ms. Sensitivity maps: sagittal plane, TE/TR $= 10/500$ ms, FA $= 30°$, BW $= 62.5$ kHz, FOV $= 240 \times 240 \times 100$ mm^3, matrix $60 \times 60 \times 20$. A high resolution T1-weighted 3D volume was also acquired for each subject for anatomical localization ($256 \times 256 \times 128$ matrix, voxel size = $0.9 \times 0.9 \times 1.2$ mm^3) as shown in Fig. 2(b)-(c).

C. fMRI data analysis

For ease of interpretation and validation, we implemented a classical slow event-related fMRI paradigm which studies occipital responses to presentation of alternative contrast checkerboard.

The five healthy subjects gave their written informed consent and this study was approved by a local ethical committee for biomedical research. Two sessions of a slow visual event-related paradigm were acquired for each subject. The stimulus was a black and white contrast reversing checkerboard with

a 20-ms period, which appears during 80 ms, followed by a 24.67-ms rest period (ISI = 24.75 s). One session consisted of 20 trials of the stimulus. All series were corrected for subject motion with SPM2 (`www.fil.ion.ucl.ac.uk`). No spatial smoothing was performed. Response magnitudes for each voxel were estimated using a general linear model with a canonical Hemodynamic Response Function (HRF) and its first derivative as regressors. A Fisher (F) test was performed to assess significance. 3D superimpositions with anatomical data were obtained with Anatomist (`http://brainvisa.info`) as shown in Fig. 2(b). For illustrative purpose, we report activations for one subject in Fig. 2(c) that were detected both in occipital cortex and cerebellum. We obtained quite reproducible activations across subjects. Fig. 3 also depicts voxel-based HRF estimates that were computed by selective averaging in voxels eliciting an activation from the raw time courses.

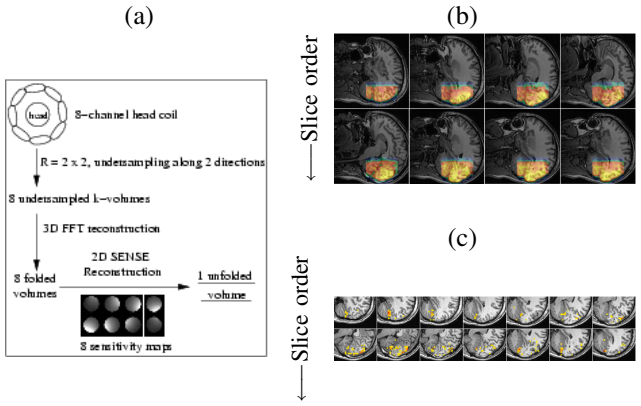

Fig. 2. **Localized Parallel EVI imaging sequence. (a)**: sketch summarizing the parallel reconstruction stragegy based on 2D SENSE unwarping technique. **(b)**: anatomical localization of zoomed EVI BOLD data. **(c)**: visual activations detected in EVI datasets (single subject) superimposed on anatomical data.

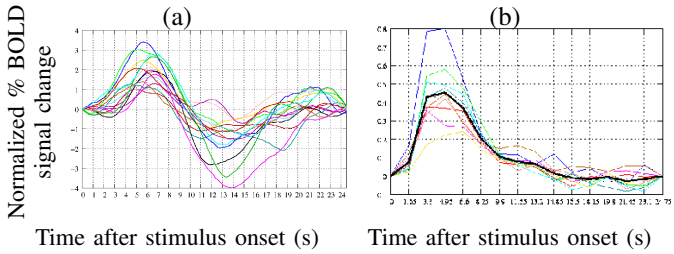

Fig. 3. **Comparison of brain dynamics seen in EVI and EPI BOLD sequences.(a)**: voxel-based HRF estimates from the parallel localized EVI sequence. **(b)**: corresponding HRF estimates from the EPI sequence for the same subject.

In parallel EPI fMRI acquisitions, regularization of parallel reconstruction generally increases the functional Contrast to Noise Ratio, through a noise reduction larger than the contrast reduction. This increase of CNR mechanically results in an increased sensitivity to the BOLD contrast. This effect has also been observed in parallel EVI: median statistical scores increase when the regularization parameter is increased. Nevertheless, this improvement slows down at high regularization factors, as also observed in [47], since the regularization condition becomes predominant over the accuracy of the reconstruction. Therefore an optimal value of λ^2 has been determined from the GLM-based analysis ($\lambda^2 \approx 0.01$).

IV. Results

A. Scaling and Multifractal: fMRI data analysis

In the present work, the ensuing goal is twofold: First, validation of the existence of scaling in the analyzed data and estimation of the MF parameters; Second, differentiation of evoked and ongoing brain activity in terms of scaling behaviors. This has never been addressed in the fMRI literature using the WLMF approach. For doing so, we statistically compare MF parameters estimated from raw motion-corrected fMRI time series acquired during activation and resting runs from selected regions of interest (ROI). Importantly, these ROIs have been identified on each subject separately from the uniquely relevant F-contrast $c = [1, 1, 0]$ to detect activations in the above mentioned SPM2 analysis. The extracted SPM clusters have been corrected for multiple comparisons and thresholded below 5 % in corrected p-value and above 5 voxels in spatial extent (up to 25 voxels). Note that the number of SPM clusters R varies from one subject to the other.

1) Scaling in fMRI data?: The first major issue lies in assessing whether the data possess scaling properties or not. To do so, one can naturally compare the power spectral density (PSD) estimate (obtained from an averaged periodogram) and the so-called log-scale diagram (LD) defined as j *vs* $\log_2(2^j S(j, q = 2))$ (cf. [28] and Section II). Using Eq. (7), both estimates can be superimposed for comparison purposes. PSD, LD and superimposition are plotted in Fig. 4 together with the time course of a voxel chosen in R_2 (and labeled $Y(t)$ for consistency with notations in Section II-C). Both the LD and PSD plots show clear power law behaviors existing over times ranging from the second to the minute. These are clear evidences in favor of the existence of scaling properties in data over this range of scales. Equivalent plots and conclusions can be drawn for each voxel of the different ROIs confirming that scaling actually exists in the analyzed data.

2) Scaling versus Non-Stationarity ? : However, Fig. 4(a) and Fig. 5(a) show that $Y(t)$ also possesses a low frequency trend. Such a very slow oscillation exists for most of the voxels under analysis. Their orders of magnitude may however significantly vary in space as may the involved range of low frequencies. These trends can be read as non stationary shifts of the mean superimposed on stationary fluctuations. Because very low frequency oscillations can naturally be modeled as $1/f$-processes, it has been claimed in the literature that the scaling observed on data may only correspond to spurious artifacts caused by non stationarities. However, it has been previously shown that wavelets brings substantial robustness in the analysis of scaling and in disentangling true scaling behavior from slow non stationarities or trends. More precisely, it enables to correctly estimate the scaling parameters when non stationarities are superimposed to a true scaling behavior and conversely to discriminate non stationarities that may be confused with scaling when using standard spectral analysis tools. This has been explained in detail in other contexts

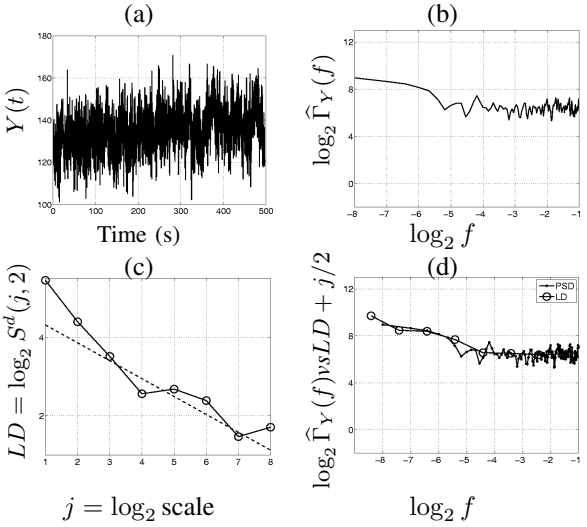

Fig. 4. **Scaling in data. (a)**: typical time course $Y(t)$ of the fluctuations recorded in a voxel of R_1 during the visual paradigm; **(b)**: corresponding PSD estimate; **(c)**: corresponding wavelet LD plot; **(d)**: comparison of the PSD with the suitably renormalized LD highlighting the superimposition of the power law behaviors and of the scaling ranges.

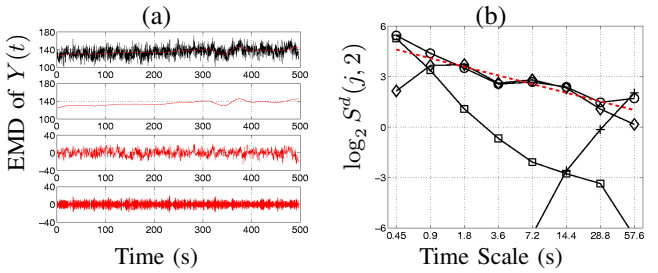

Fig. 5. **Scaling *vs* Non-Stationarity Analysis.** (a): fMRI time series for an activating voxel, and its EMD based separation into (from top to bottom) low, medium and high frequency components. (b): the corresponding LDs (time series: 'o', LF: '+', mF: '$\diamond$', HF: '$\square$').

in [28, 30, 32–34] and will therefore not be further discussed here. Instead, we chose to further examine the issue of trend versus scaling discrimination by making use of a recent tool, the *Empirical Mode Decomposition* (EMD) [49]. The precise definition and details of EMD cannot be given here for sake of space, the reader is referred to the excellent tutorial paper [50]. The main output of EMD consists of the fact that the analyzed data can be split into various components.

We chose to split data into 3 components: a very low frequency trend (LF), a medium frequency signal (mF) and a high frequency noise (HF), as illustrated in Fig. 4(a). Both the LF trend and the HF noise may either alter the analysis of scaling or be confusingly associated to scaling, as commonly speculated in the literature.

LDs are computed independently for the entire original time series, and the three components. They are superimposed in Fig. 5(b), clearly showing that the scaling, and scaling range, observed on the entire time series are neither caused by the LF nor by the HF components but are rather entirely due to fluctuation (mF component). The trend in itself also exhibits a power law behavior in the LD plot, but in a much coarser range of scales (beyond the minute) and with a clearly different scaling exponent. Moreover, when N (the number of vanishing moments of ψ_0) is increased the scaling exponent that can be estimated from the trend varies in a proportional and trivial manner. This is not the case for the scaling exponent estimated from the fluctuation (mF) component that remains (quasi-) constant when N is varied, a significant experimental proof in favor of the actual existence of scaling in data (see [28] for further details). Moreover, we can check that the scaling exponents estimated on the entire time series and on the mF component closely match. These analyses unambiguously disentangle true scaling properties from non stationary superimposed trends or high frequency noise corruption.

The analyses reported here clearly shows that the fMRI data under analysis possesses scaling properties, within scales that range from the second to the minute and that are not related to slow trends, whatever their origins.

3) Multifractality?: Now that the existence of scaling in data is established, let us proceed, in a second step, to a more detailed and quantitative multifractal analysis. We apply the WLMF analysis procedure, as described in Section II-D, to the voxel-based mF signal component for all voxels in the identified SPM clusters. Because the Leader approach requires a positive regularity of the time series (*cf.* [27, 40]), analysis procedures are applied to the *cumulated sum* of the observed time series (*i.e.,* labeled as X in the notations of Section II) rather than to the time series Y itself.

The corresponding Leader-based LDs (LLDs) show clear scaling behaviors holding for $3 \leqslant j \leqslant 6$, i.e., for time scales ranging from 1.5 to 15s that slightly differ between rest and activation datasets. This is illustrated in Fig. 6 for a voxel (chosen as representative) both during the visual experiment and resting state. The corresponding scaling exponents $\zeta(q)$ and MF spectrum $D(h)$ are compared in Fig. 7(a)-(b), respectively. It shows that, for both the visual experiment and the resting state, the departure of the $\hat{\zeta}(q)$s from a linear behavior in q is weak, yet clear (or equivalently that the $\hat{D}(h)$ is narrow, yet not collapsing onto one single point). This hence leads to the conclusion that the analyzed data possess a weak yet significant and measurable multifractality. Akin to [18], we have also regressed out the modelled BOLD response in order to illustrate the presence of multifractality on the residuals. As shown in Fig. 8(a), the main difference observed between the scaling parameters $(\hat{c}_1^L, \hat{c}_2^L)$ computed from the residuals (blue curve) and the original activated time series (red curve) depicted in Fig. 6 (a) lies in the long-range correlation structure, ie. in $\hat{c}_1^L$, which specifies the amount of self-similarity. The mode of the residual-based multitfractal spectrum has actually shifted away to the left and appears closer to the MF spectrum we obtained from the resting state time series in the same voxel (black curve), which is depicted in Fig. 6 (d). This confirms therefore that multifractality is not specific to activated voxels or to evoked activity and mainly brings information relative to ongoing activity, what is usually called "noise" in the fMRI literature [14, 18, 21]. Also, Fig. 8(b) shows the corresponding multifractal spectra computed in a less activated voxel as compared to Fig. 8(a) ($T_{\rm val} = 3.52$ vs. $T_{\rm val} = 5.1$). Hence, the position of the mode seems to depend on the activity level. This should

be further investigated by a massive voxel-based analysis of the residuals.

The comparison results between ongoing and evoked activity are further confirmed by the analysis of the plots of the log-cumulant structure functions, $C^L(j,p)$, defined in Eq. (14), in Fig. 9 (from which $\hat{c}_1^L$ and $\hat{c}_2^L$ are estimated). The estimated $C^L(j,2)$ clearly possesses a (negative) non zero slope hence yielding a negative $\hat{c}_2^L$. Let us emphasize that the more negative $\hat{c}_2^L$, the stronger the experimental evidence in favor of multifractality.

Now that an experimental scaling range has been conclusively determined, $1.5 \leq 2^j T_s \leq 15$s, a systematic estimation of the multifractal parameters can be performed for each voxel for both the the visual experiment and resting state. Scaling exponents $\zeta(q)$, the multifractal spectrum $D(h)$ or the log-cumulant c_p accounting theoretically equivalently for the scaling content of the analyzed data, we chose to concentrate on the log-cumulant c_1^L, c_2^L only: c_1^L mostly amounts to the self-similarity characterization, while c_2^L measure the deviation from pure self-similarity hence the impact of the multifractal component of the data.

These systematic analyses yield the following conclusions. For parameter c_1, we observe that it consistently takes values in the range $0.50 \leqslant c_1 \leqslant 1$ (cf. Fig. 11), both for ongoing and evoked brain activity, hence confirming the relevance of the LRD paradigm to characterize fMRI time series correlations. Also, we note that activation systematically (for all subjects and all ROIs) results in an increase in c_1, from the range $0.50 \leqslant c_1 \leqslant 0.75$ for ongoing activity to the range $0.70 \leqslant c_1 \leqslant 0.95$ for evoked activity. Activation hence induces an increase of the LRD strength and impact. This is consistent with findings reported in [21]. For parameter c_2, the situation is more intricate, partly due to the fact that estimation is by far more difficult [42]. Nevertheless, we observe that, in some cases, activations coincide with an increase in c_2, from negative to close to 0 values, hence with a decrease in multifractality (cf. Fig. 12), while in others there is no significant modification in c_2 between both data types.

Therefore, a key result of these scaling analyses consists of the fact that compared to the resting state, the visual experiment induces a clear, sharp and systematic increase in the LRD parameter, while it either produces a decrease in the degree of multifractality or does not alter it. The statistical significance of these results is further assessed by means of statistical tests in Section IV-B.

4) Wavelet coefficients vs. Leaders: To further discuss whether one should prefer to use wavelet coefficients or wavelet Leaders (i.e., WCMF or WLMF) for scaling analysis, one can compare estimations for c_1 and c_2 in Fig. 10. For c_1, one observes that the dispersion (or confidence interval size) for the $\hat{c}_1^d$ is larger than that of the $\hat{c}_1^L$ but not significantly so. For c_2, the situation is very different, the dispersion of $\hat{c}_2^L$ is dramatically diminished (by one order of magnitude) compared to that of $\hat{c}_2^d$. This is in perfect agreement with the analyses reported in [42] and yields the following conclusions of major practical importance. As long as scaling are modeled in terms of self-similarity only (i.e., one assumes that the sole parameter c_1 describes scaling), statistical performance are slightly better for Leaders compared to coefficients, at the price though of extra difficulties in selecting the range of scales where to perform the linear regressions. Therefore, Leaders and coefficients should be used jointly and collaboratively. When it comes to estimate c_2, hence scaling related to multifractal properties, only the WLMF should be used as the confidence interval sizes obtained with WCMF are so large that no conclusion can be drawn. Practically, in the statistical tests performed in Section IV-B below, this induces that it is strictly not possible to detect any change in c_2 when one uses wavelet coefficients, while Leader based tests clearly show a number of changes. Relevant and accurate estimations of c_2, with reduced confidence interval sizes, therefore constitute the major benefits of the use of Leaders in this context. Also, let us note that tests based on wavelet coefficients would miss a number of changes in c_1, despite their effect being net, that are clearly seen using Leader based tests.

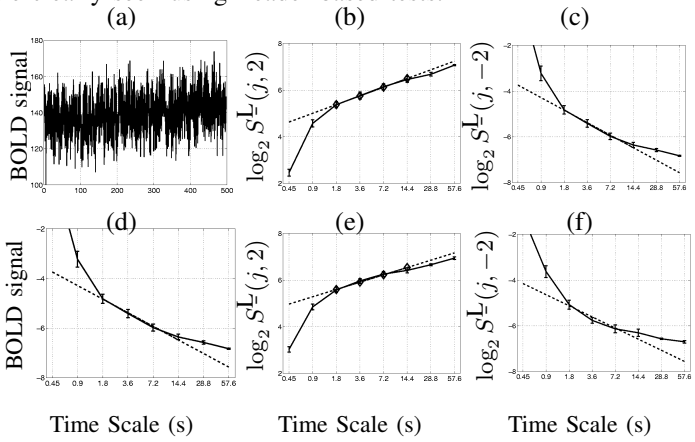

Fig. 6. **Leader based Multifractal Analysis. (a)**: fMRI signal acquired during the visual experiment. **(b)-(c):** The log-scale diagrams computed for $q = 2$ **(b)** & $q = -2$ **(c)** from the time series depicted in (a). They show a clear scaling range, from 1.5 to 15s. **(d)**: fMRI signal acquired during resting state in the same voxel as in (a). **(e)-(f):** Corresponding Log-scale diagrams computed for $q = \pm 2$ showing also a scaling phenomenon ranging from 1.5 to 15s.

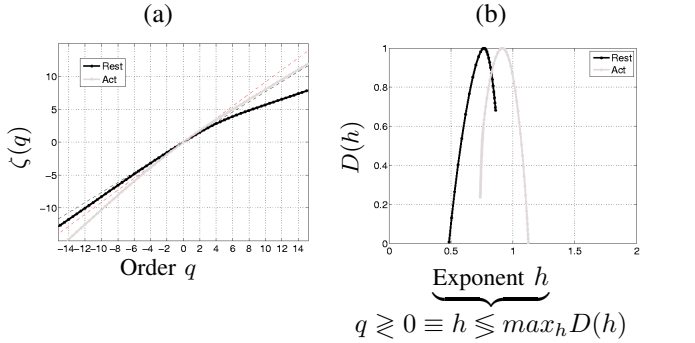

Fig. 7. **Leader based Multifractal spectrum.** Computation of the pair $(\zeta(q), D(h))$ from two fMRI time series corresponding to activation (light gray) and resting state (black) datasets in the same voxel.

B. Region-based hypothesis testing

The next goal consists in assessing the statistical significance of the observed difference in every cluster R_i between $\mathrm{med}[\widehat{\boldsymbol{c}}_p^{\mathrm{r}}]$ and $\mathrm{med}[\widehat{\boldsymbol{c}}_p^{\mathrm{v}}]$. We use nonparametric tests and robust

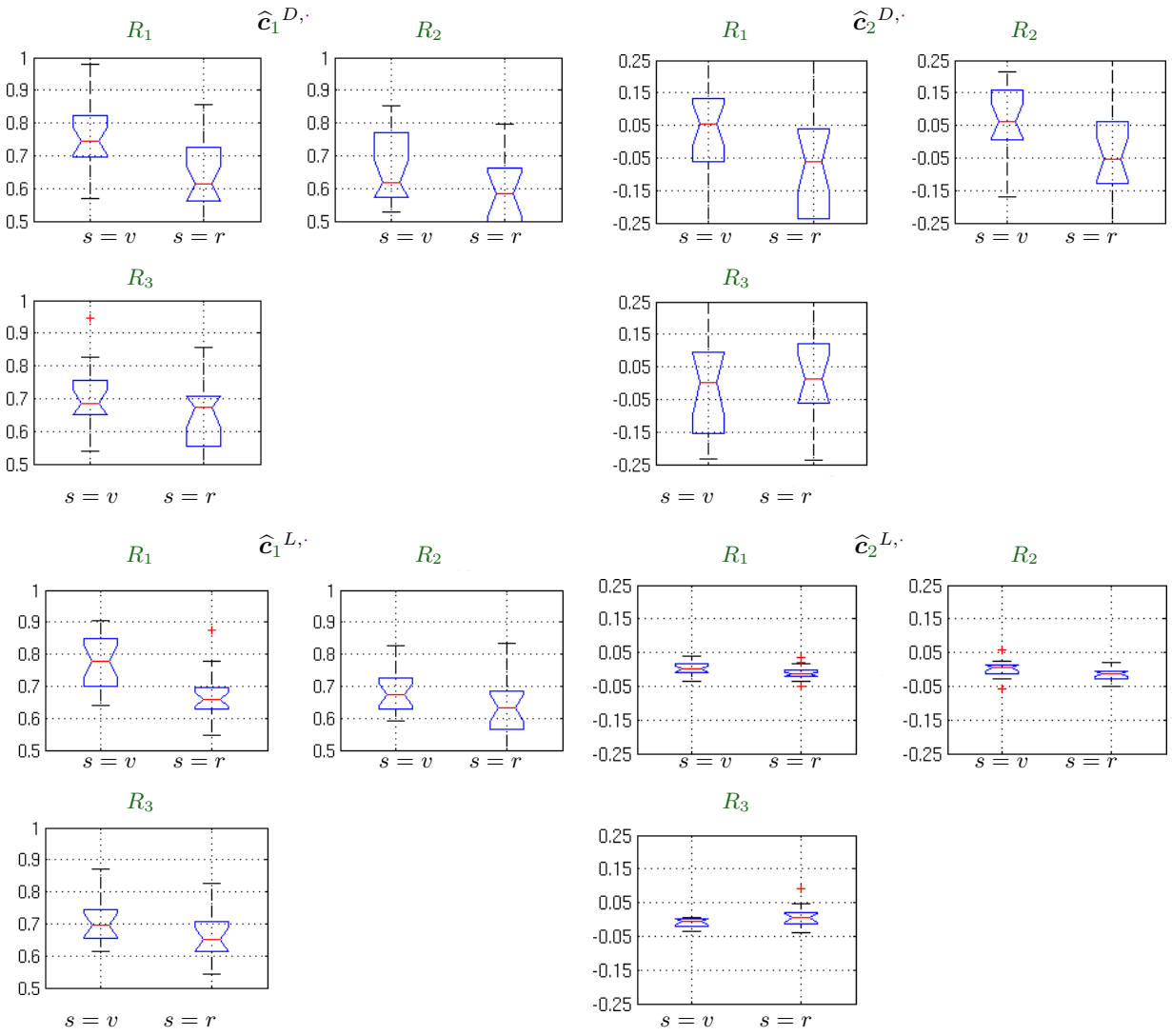

Fig. 10. **Statistical comparison of evoked v.s. ongoing activity**: estimation of c_1 and c_2 from the wavelet coefficients (top rows) and wavelet Leaders (bottom rows) for Subject 2. Each panel corresponds to a region (R_1 to R_3) identified as a significant SPM-cluster during the visual experiment. In each ROI, the box-plot shows the *median* of the voxel-dependent cumulant estimates based upon the wavelet coefficients ($\widehat{\boldsymbol{c}}_1^{d,s}, \widehat{\boldsymbol{c}}_2^{d,s}$) and Leaders ($\widehat{\boldsymbol{c}}_1^{L,s}, \widehat{\boldsymbol{c}}_2^{L,s}$) for visual ($s = v$) and rest ($s = r$) sessions, respectively.

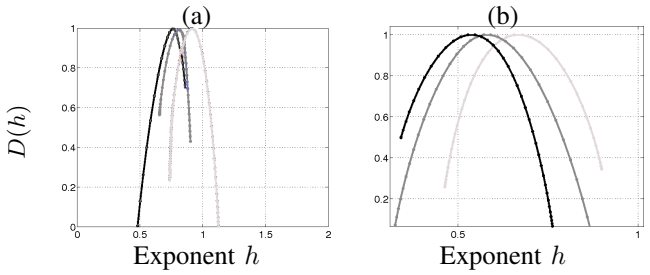

Fig. 8. **Leader based Multifractal spectra.** Comparison of multifractal spectra computed in a strongly (a) and weakly (b) activated voxels from the original time series (light gray) and the residuals (dark gray). The multifractal spectra $D(h)$ obtained in the same voxel during the resting state acquisition period are reported in black.

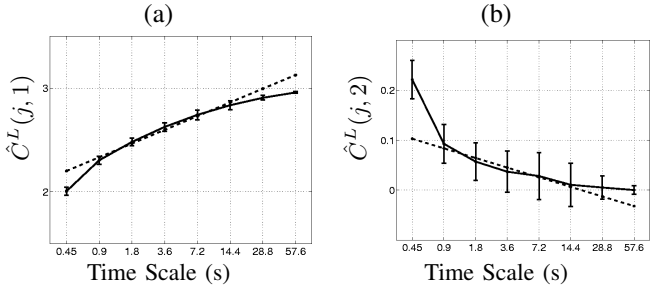

Fig. 9. **Log-Cumulants:** Estimated log-Leaders Cumulant functions $\hat{C}^L(j,p)$ for $p = 1$ (a) and $p = 2$ (b). From these linear behaviors in j, one estimates the classifiers $\hat{c}_1^L, \hat{c}_2^L$.

statistics as there is no evidence that the scaling parameters are normally distributed across voxels for a given ROI. In such a case, one usually resorts to robust decision statistics (*e.g.,* to the Wilcoxon's signed rank (WSR) statistic), whose correct specificity control (control of false positives) can be correctly handled in the permutation testing framework [51, 52]. Here, robustness means that the influence of outliers on statistics remains bounded. Precisely, we perform the following *two-*

sided tests :

$$H_{0,p}^{\mathrm{r}\neq\mathrm{v}} : \mathrm{med}[\widehat{\boldsymbol{c}}_p^{\mathrm{r}}] = \mathrm{med}[\widehat{\boldsymbol{c}}_p^{\mathrm{v}}], \quad \forall\, p = 1 \text{ or } 2, \qquad (17)$$

which amount to testing whether the difference between the matched samples $\widehat{\boldsymbol{c}}_p^{\mathrm{r}}$ and $\widehat{\boldsymbol{c}}_p^{\mathrm{v}}$ comes from a distribution whose *median* $\mathrm{med}[\widehat{\boldsymbol{c}}_p^{\mathrm{r}-\mathrm{v}}] = \mathrm{med}[\widehat{\boldsymbol{c}}_p^{\mathrm{r}} - \widehat{\boldsymbol{c}}_p^{\mathrm{v}}]$ is zero.

Fig. 11 shows the corresponding WSR statistic p-values and validates that the observed increase in c_1 is quasi-systematically significant across subjects. Again, for c_2, the results reported in Fig. 12 are less clear, as significance of the changes varies with ROIs and subjects. However, results, over the entire datasets indicate a slight shift tendency in c_2 from negative to close to 0 values, when the test is significant. This confirms a global effect of reduction of multifractality under activation.

V. Discussion and perspectives

In this contribution, we have analyzed the scaling and multifractal properties of EVI fMRI data acquired during a resting state and a slow visual event-related activation protocol. To do so, we made use of the most recent theoretical and practical developments in multifractal analysis. They are based on wavelet Leaders instead of wavelet coefficients. Also, we clearly detailed and entangled the often confused relations between the most common stochastic process models used to account for scaling, namely $1/f$-, long range dependent, self-similar and multifractal processes. The various parameters commonly involved in scaling description are also clearly related, and the analysis and estimation procedures are detailed. The use of wavelet coefficients and wavelet Leaders is compared to the benefits of the latter.

Using this careful methodology and powerful estimation tools, we provided significant evidence for the presence of scaling in the analyzed fMRI datasets, for the five participants, that can in no way be confused with non stationarities or low frequency oscillating trends, which were also present in data, yet superimposed to true scaling. Also, we established that this scaling properties should be related to both long memory in time and multifractality (in agreement with [14, 21]). Given our acquisition parameters, especially the deliberate choice of a large scan number, scaling parameters are estimated with a high degree of precision and thus are reliable.

As concluded from Section IV-B, we demonstrated the existence of relationships between the scaling parameter estimates and the congruence between the ROIs and the data under consideration. Our findings show that activation induces a clear and systematic increase in the long range dependence (or self-similarity) c_1 parameter together with a (less clear and less systematic) decrease of the multifractality c_2 parameter. Interestingly, the former is connected to additive random walk and linear filtering while the latter is rather related to non-linear mechanisms. Therefore, the parameter c_2 that characterizes deviations from self-similarity can be thought of as a measure of the importance of non-linear effects in neurophysiological mechanisms. Our results suggest that activation tends to reduce their impact: this could be expected given the very simple nature of our paradigm. Also, in future works, we will take advantage of the use of non parametric bootstrap in multifractal analysis that enables not only to produce an estimate but also a confidence interval for each voxel independently [39]. This is likely to significantly improve the accuracy of the change detection tests and make feasible the use of mixed effect models for region-based inference.

This preliminary study needs to be further developed if one wants to consider multifractal attributes as putative classifiers of brain activity. In particular, to achieve a reliable model-free analysis, which is able to detect and localize task-related activity, we must explore true contrasts in the sense of comparing brain activity induced by different external stimuli on the same time series using these multifractal attributes as stimulus markers. In contrast to [21], this should be investigated in event-related protocols, for which the BOLD signal fluctuations in time and frequency is much more complex. In such cases, we could find out more multifractal situations, for instance in regions eliciting habituation or learning phenomena as those described in [53]. To this end, we are currently exploring whole brain analysis blind to the use of any a priori model-based detection. On our first experiment on a single subject (results not shown) we observe that MF parameters are primarily influenced in brain regions involved in the experimental paradigm and also that these parameters remain quite unchanged in other regions when comparing the activation dataset to the resting state one. This has to be confirmed and reproduced on more datasets i.e. on more subjects.

Repeating such analyses to the whole brain and not specifically to activating clusters may make the method more relevant for exploring long range task-related spatial interactions based upon the scaling properties, as suggested in [19]. Hence, the whole-brain extension of the proposed approach will offer the possibility to study functional connectivity based on resting-state functional fMRI data and to explain how such long range interactions are modulated by external stimulation. Therefore, this study shall fulfill several important objectives for the understanding of brain structure and function:

- Elucidate the structure of spontaneous activity seen in fMRI as a marker of functional connectivity: the correlation of the spontaneous activity between distant regions observed in fMRI reflects the functional relationship between these distant regions [54]. This is related to the concept of functional integration [55] and provides the structure of some fundamental subdivisions of the brain (see e.g. [56]).
- Disentangle the relationship with anatomical connectivity: it is not completely clear whether the spatial structure of spontaneous activity reflects the spatial structure of the anatomical connectivity or whether there are other components that could be identified. Such a comparison becomes possible because diffusion MRI provides an in vivo access on human brain anatomical connectivity structure [57].
- Understand the relationship between ongoing and evoked activity: Some studies have proposed that evoked activity (i.e. the activity resulting from an input stimulus) would superimpose linearly with spontaneous activity [58] while other studies insist that spontaneous activity could be

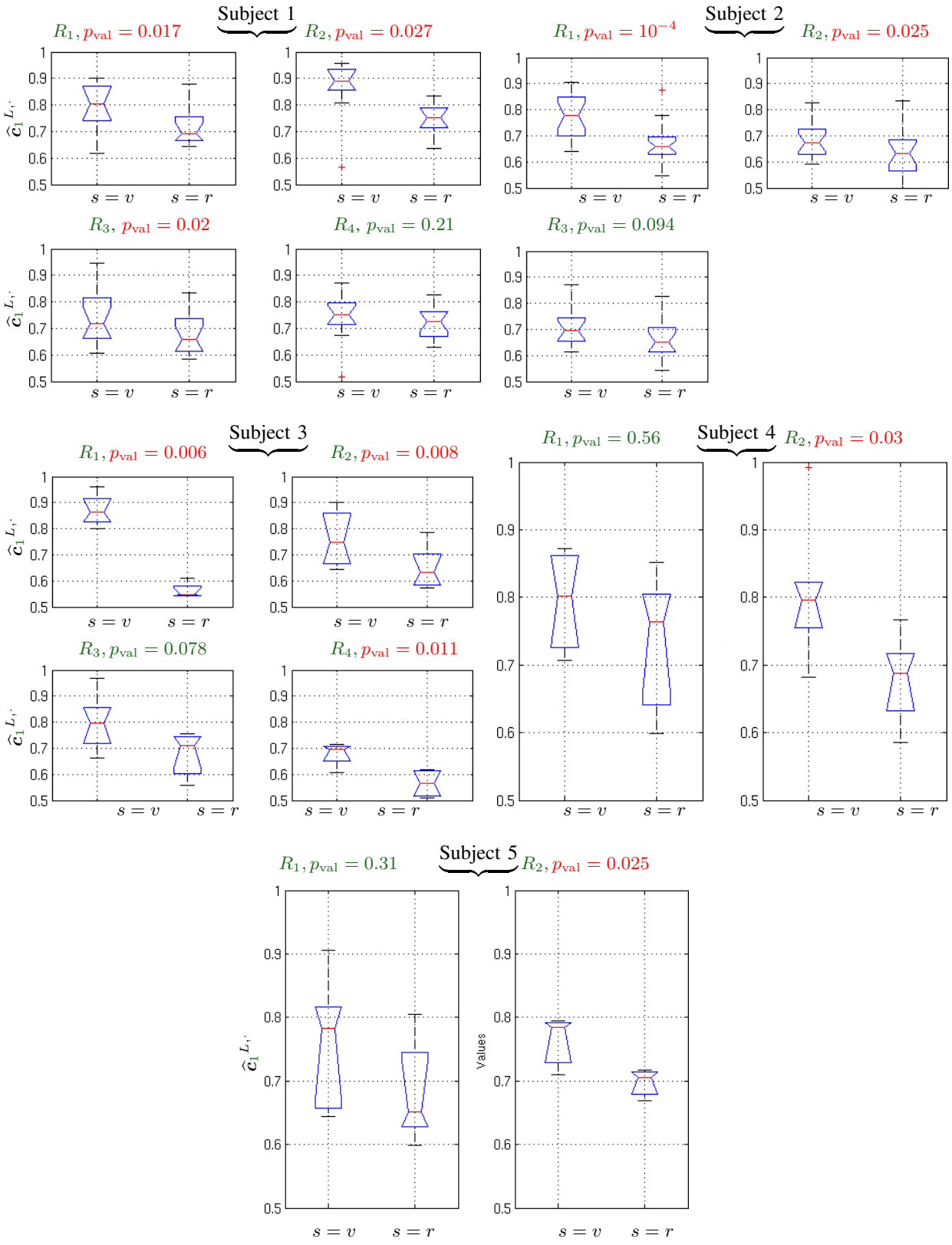

Fig. 11. **Statistical comparison of evoked v.s. ongoing activity**: estimation of c_1, *i.e.,* the linear component of $\zeta(q)$. Each panel corresponds to a region (R_1 to R_4) identified as a significant SPM-cluster during the visual experiment. This explains why the number of regions varies across subjects. In each ROI, the box-plot shows the *median* of the voxel-dependent WLMF estimates $\widehat{\boldsymbol{c}}_1^{\mathrm{s}}$ for visual ($s = v$) and rest ($s = r$) sessions, respectively. The WSR statistic p-values are displayed at the top of each panel *i.e.,* for each region. Red marks show significant changes between resting state and visual experiment at 5%.

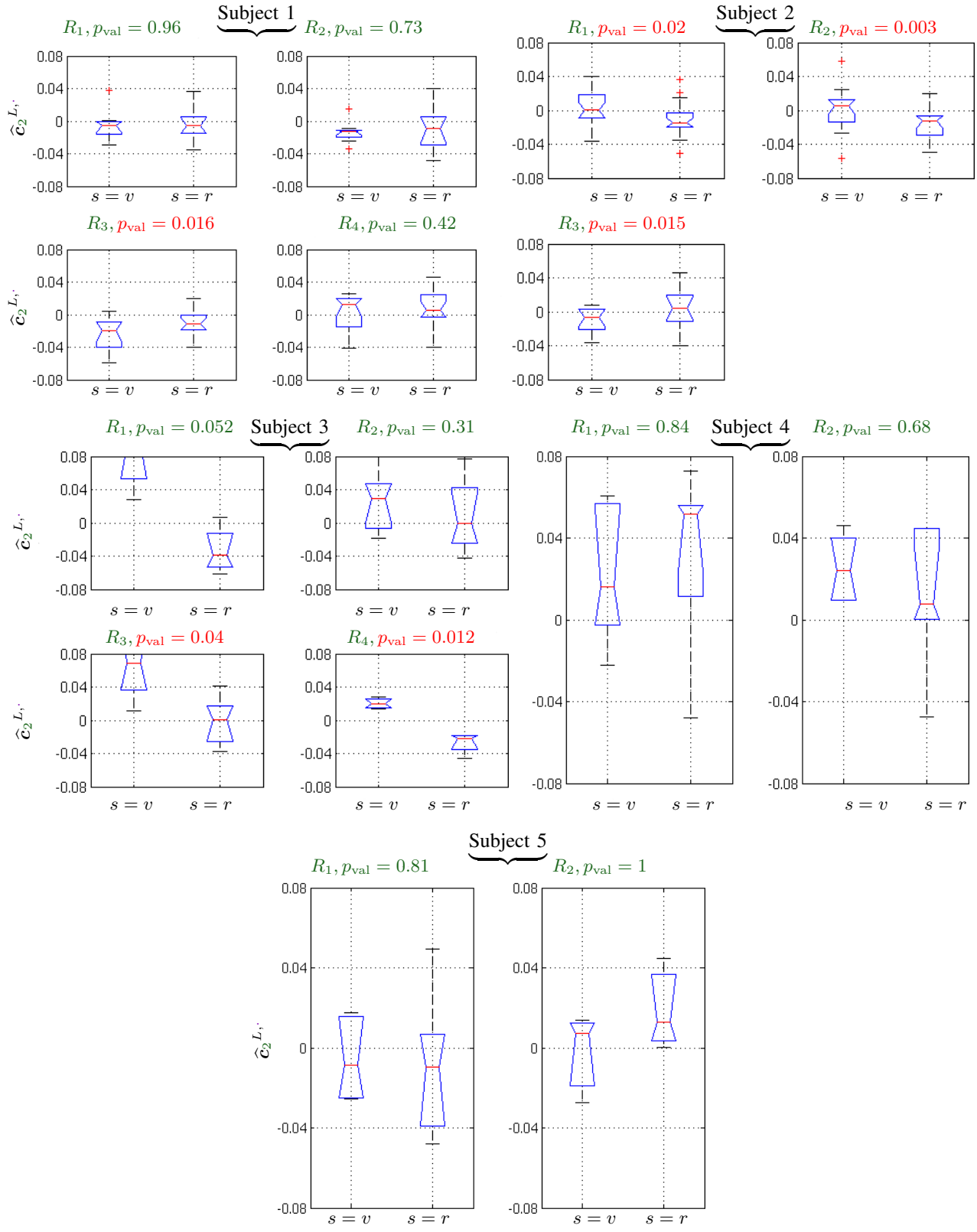

Fig. 12. **Statistical comparison of evoked v.s. ongoing activity**: estimation of c_2, *i.e.,* the quadratic component of $\zeta(q)$. Each panel corresponds to a region (R_1 to R_4) identified as a significant SPM-cluster during the visual experiment. This explains why the number of regions varies across subjects. In each ROI, the box-plot shows the *median* of the voxel-dependent WLMF estimates $\widehat{\boldsymbol{c}}_2^{\,s}$ for visual ($s = v$) and rest ($s = r$) sessions, respectively. The WSR statistic p-values are displayed at the top of each panel *i.e.,* for each region. Red marks show significant changes between resting state and visual experiment at 5%.

predictive of the behavior [59]. These two points of view require further assessment.

- Compare the spontaneous activity in different populations (patients and controls). By considering functional connectivity as a measure that characterizes the integration of brain structures into networks, one can use it for comparing different kinds of populations: infants versus adults, normal subjects versus patients [60]. A particular interest in the study of resting-state networks is that the connectivity or integration of these networks are not confounded by different levels of the subjects in the performance of task.

Currently, many approaches have been proposed to study resting-state brain connectivity, mainly bivariate approaches, based on distant correlations of the signal [61–63], and multivariate approaches, mainly based on ICA [56, 64] and clustering [65, 66]. Our feeling is that brain connectiviy analysis based upon multifractal attributes would help discriminate linear from non-linear inter-dependency and that the MF methodology defines a framework for studying how network activity is modulated between resting and stimulation periods.

ACKNOWLEDGMENT

This project has been partly funded by the French research agency (ANR), grant number ANR-005-MMSA-0014-03 (OPTIMED project).

REFERENCES

[1] M. McKeown, "Detection of consitently task-related activation in fMRI data with hybrid independent component analysis", *Neuroimage*, vol. 11, pp. 24–35, 2000.

[2] V. Calhoun, T. Adali, G. Pearlson, and J. Pekar, "Spatial and temporal independent component analysis of functional MRI data containing a pair of task-related waveforms", *Hum. Brain Mapp.*, vol. 13, pp. 43–53, 2001.

[3] C. Beckmann and S. Smith, "Probabilistic independent component analysis for functional magnetic resonance imaging", *IEEE Trans. Med. Imag.*, vol. 23, pp. 137–152, 2004.

[4] E. Zarahn, G. K. Aguirre, and M. D'Esposito, "Empirical analysis of BOLD fMRI statistics. I. Spatially unsmoothed data collected under null-hypothesis conditions", *Neuroimage*, vol. 5, pp. 179–197, Apr. 1997.

[5] E. Bullmore, J. Fadili, V. Maxim, L. Şendur, B. Whitcher, J. Suckling, M. Brammer, and M. Breakspear, "Wavelets and functional magnetic resonance imaging of the human brain", *Neuroimage*, vol. 23, pp. S234–S249, 2004.

[6] R. M. Birn, P. A. Bandettini, R. W. Cox, A. Jesmanowicz, and R. Shaker, "Magnetic field changes in the human brain due to swallowing or speaking", *Magn. Reson. Med.*, vol. 40, pp. 55–60, 1998.

[7] J. Diedrichsen and R. Shadmehr, "Detecting and adjusting for artifacts in fMRI time series data", *Neuroimage*, vol. 27, pp. 624–634, Sep. 2005.

[8] P. L. Purdon and R. M. Weisskoff, "Effect of temporal autocorrelation due to physiological noise and stimulus paradigm on voxel-level false-positive rates in fMRI.", *Hum. Brain Mapp.*, vol. 6, pp. 239–249, 1998.

[9] L. Frank, R. Buxton, and E. Wong, "Estimation of respiration induced noise fluctuations from undersampled multislice fMRI data", *Magn. Reson. Med.*, vol. 45, pp. 635–644, 2001.

[10] G. Kruger and G. Glover, "Physiological noise in oxygenationsensitive magnetic resonance imaging", *Magn. Reson. Med.*, vol. 46, pp. 631–637, 2001.

[11] E. Bullmore, C. Long, J. Suckling, J. Fadili, G. Calvert, F. Zelaya, T. Carpenter, and M. Brammer, "Colored noise and computational inference in neurophysiological (fMRI) time series analysis", *Hum. Brain Mapp.*, vol. 12, pp. 61–78, 2001.

[12] F. G. Meyer, "Wavelet-based estimation of a semi-parametric generalized linear model of fMRI time series", *IEEE Trans. Med. Imag.*, vol. 22, pp. 315–322, Mar. 2003.

[13] C. Long, E. N. Brown, L. W. C. Triantafyllou, I. Aharon, and V. Solo, "Nonstationary noise estimation in functional MRI", *Neuroimage*, vol. 28, pp. 890–903, Dec. 2005.

[14] J. Fadili and E. Bullmore, "Wavelet-generalized least squares: A new BLU estimator of linear regression models with 1/f errors", *Neuroimage*, vol. 15, pp. 217–232, Jan. 2002.

[15] L. Huaien and S. Puthusserypady, "fMRI data analysis with nonstationary noise models: a Bayesian approach", *IEEE Trans. Biomed. Eng.*, vol. 54, pp. 1621–1630, Sep. 2007.

[16] M. A. Burock, R. L. Buckner, M. G. Woldorff, B. R. Rosen, and A. M. Dale, "Randomized event-related experimental designs allow for extremely rapid presentation rates using functional MRI.", *Neuroreport*, vol. 9, pp. 3735–3739, Nov. 1998.

[17] D. Leopold, Y. Murayama, and N. Logothetis, "Very slow activity fluctuations in monkey visual cortex: implications for functional brain imaging.", *Cereb. Cortex*, vol. 13, pp. 422–33, Apr 2003.

[18] S. Thurner, E. Windischberger, C. Moser, P. Walla, and M. Barth, "Scaling laws and persistence in human brain activity", *Physica A*, vol. 326, pp. 511–521, 2003.

[19] V. Maxim, L. Sendur, J. Fadili, J. Suckling, R. Gould, R. Howard, and E. Bullmore, "Fractional Gaussian noise, functional MRI and Alzheimer's disease.", *Neuroimage*, vol. 25, pp. 141–158, mar 2005.

[20] K. Linkenkaer-Hansen, S. Monto, H. Rytsala, K. Suominen, E. Isometsa, and S. Kahkonen, "Breakdown of long-range temporal correlations in theta oscillations in patients with major depressive disorder.", *J Neurosci*, vol. 25, pp. 10131–10137, Nov 2005.

[21] Y. Shimizu, M. Barth, C. Windischberger, E. Moser, and S. Thurner, "Wavelet-based multifractal analysis of fMRI time series.", *Neuroimage*, vol. 22, pp. 1195–1202, Jul 2004.

[22] A. Arneodo, E. Bacry, and J. Muzy, "Solving the inverse fractal problem from wavelet analysis", *Europhys. Lett.*, vol. 25, pp. 479–, 1993.

[23] J.-F. Muzy, E. Bacry, and A. Arneodo, "Multifractal formalism for fractal signals. The structure function method versus the wavelet transform modulus maxima method", *Phys. Rev. E*, vol. 47, pp. 875–884, 1993.

[24] J. Lee, J. Hu, J. Gao, K. White, B. Crosson, C. Wierenga, K. McGregor, and K. Peck, "identification of brain activity by fractal scaling analysis of functional MRI data", in *30th Proc. IEEE ICASSP*, Philadelphia,, May 2005, vol. II, pp. 137–140.

[25] M.-E. Torres and P. Abry, "Comparison of different methods for computing scaling parameter in the presence of trends", in *14th BioIngineering argentin congress*, A. Cordoba, Ed., 2003.

[26] A. Arneodo, B. Audit, N. Decoster, J.-F. Muzy, and C. Vaillant, "Wavelet-based multifractal formalism: applications to dna sequences, satellite images of the cloud structure and stock market data", *The Science of Disasters*, vol. A. Bunde, J. Kropp, H. J. Schellnhuber eds., pp. 27–102, 2002.

[27] S. Jaffard, "Wavelet techniques in multifractal analysis", in *Fractal Geometry and Applications: A Jubilee of Benoît Mandelbrot, M. Lapidus et M. van Frankenhuijsen Eds., Proceedings of Symposia in Pure Mathematics*. 2004, vol. 72(2), pp. 91–152, AMS.

[28] P. Abry, P. Flandrin, M. Taqqu, and D. Veitch, "Wavelets for the analysis, estimation and synthesis of scaling data", in *K. Park and W. Willinger Eds, Self-similar Network Traffic and Performance Evaluation*. spring 2000, Wiley.

[29] C. Rabrait, P. Ciuciu, A. Ribés, C. Poupon, P. Leroux, V. Lebon, G. Dehaene-Lambertz, D. L. Bihan, and F. Lethimonnier, "High temporal resolution functional MRI using parallel echo volume imaging", *Journal of Magnetic Resonance Imaging*, vol. 27, pp. 744–753, Mar. 2008.

[30] P. Abry, P. Gonçalvès, and P. Flandrin, "Wavelets, spectrum analysis and $1/f$ processes", in *Lecture Notes in Statistics: Wavelets and Statistics*, A. Antoniadis and G. Oppenheim, Eds., 1995, vol. 103, pp. 15–29.

[31] A. M. Smith, B. K. Lewis, U. E. Ruttimann, F. Q. Ye, T. M. Sinnwell, Y. Yang, J. H. Duyn, and J. A. Frank, "Investigation of low frequency drift in fmri signal", *Neuroimage*, vol. 9, pp. 526–533, May 1999.

[32] P. Abry and D. Veitch, "Wavelet analysis of long-range dependent traffic", *IEEE Trans. on Info. Theory*, vol. 44, pp. 2–15, January 1998.

[33] D. Veitch and P. Abry, "A wavelet-based joint estimator of the parameters of long-range dependence", *IEEE Trans. on Info. Theory*, vol. 45, pp. 878–897, 1999.

[34] D. Veitch and P. Abry, "A statistical test for the time constancy of scaling exponents", *IEEE Trans. on Sig. Proc.*, vol. 49, pp. 2325–2334, 2001.

[35] P. Abry, R. Baraniuk, P. Flandrin, R. Riedi, and D. Veitch, "Multiscale nature of network traffic", *IEEE Signal Processing Magazine*, vol. 19, pp. 28– 46, 2002.

[36] G. Samorodnitsky and M. Taqqu, *Stable non-Gaussian random processes*, Chapman and Hall, New York ISBN 0-412-05171-0, 1994.

[37] R. H. Riedi, "Multifractal processes", *in: "Theory and applications of long range dependence ", eds. Doukhan, Oppenheim and Taqqu*, pp. 625–716, 2003.

[38] S. Mallat, *A Wavelet Tour of Signal Processing*, Academic Press, San Diego, CA, 1998.

[39] H. Wendt, P. Abry, and S. Jaffard, "Bootstrap for empirical multifractal analysis", *IEEE Signal Processing Mag.*, vol. 24, pp. 38–48, 2007.

[40] S. Jaffard, B. Lashermes, and P. Abry, "Wavelet leaders in multifractal analysis", in *Wavelet Analysis and Applications,T Qian, M. I; Vai, X. Yuesheng, Eds.*, Basel, Switzerland, 2006, pp. 219–264, Birkhäuser Verlag.

[41] B. Castaing, Y. Gagne, and M. Marchand, "Log-similarity for turbulent flows", *Physica D*, vol. 68, pp. 387–400, 1993.

[42] H. Wendt, S. Roux, and P. Abry, "Bootstrap for log wavelet cumulant based multifractal analysis", in *Proceedings of of EUSIPCO*, Firenze, Italy, 2006.

[43] P. Mansfield, "Multi-planar image formation using NMR spin-echoes", *J.Phys.C : Solid State Phys.*, vol. 10, pp. L55–L58, 1977.

[44] P. Mansfield, R. Coxon, and J. Hykin, "Echo-volumar imaging (EVI) of the brain at 3.0T: first normal volunteer and functional imaging results", *J. Computer Assisted Tomography*, vol. 19, pp. 847–852, 1995.

[45] W. van der Zwaag, S. Francis, and R. Botwell, "Improved echo volumar imaging (EVI) for functional MRI", *Magn. Reson. Med.*, vol. 56, pp. 1320–1327, 2006.

[46] F. Lin, T.-Y. Huang, N.-K. Chen, F.-N. Wang, S. M. Stufflebeam, J. Belliveau, L. Wald, and K. Kwong, "Functional MRI using regularized parallel imaging acquisition", *Magn. Reson. Med.*, vol. 54, pp. 343–353, 2005.

[47] A. Ribés, C. Poupon, C. Rabrait, D. Le Bihan, and F. Lethimonnier, "Tikhonov regularisation optimisation for PreLearn: effects on the detection of activation in functional MRI", in *Proc. 15th ISMRM*, Berlin, 2007, p. 1757.

[48] K. F. King, "SENSE image quality improvement using matrix regularization", in *Proc. 9th ISMRM*, Glasgow, 2001, p. 1771.

[49] N. Huang, Z. Shen, S. Long, M. Wu, H. Shih, Q. Zheng, N. Yen, C. Tung, and H. Liu, "The empirical mode decomposition and the hilbert spectrum for nonlinear and non-stationary time series analysis", *Proc. R. Soc. Lond. A*, vol. 454, pp. 903–995, 1998.

[50] P. Flandrin and P.Gonçalves, "Empirical mode decomposition as data-driven wavelet-like expansions", *Int. J. Wav. Multires. Info. Proc.*, vol. 2, pp. 477–496, Dec. 2004.

[51] S. Mériaux, A. Roche, G. Dehaene-Lambertz, B. Thirion, and J.-B. Poline, "Combined permutation test and mixed-effect model for group average analysis in fMRI.", *Hum. Brain Mapp.*, vol. 27, pp. 402–410, May 2006.

[52] T. Nichols and S. Hayasaka, "Controlling the Familywise Error Rate in Functional Neuroimaging: A Comparative Review", *Statistical Methods in Medical Research*, vol. 12, pp. 419–446, 2003.

[53] G. Dehaene-Lambertz, S. Dehaene, J.-L. Anton, A. Campagne, P. Ciuciu, G. P. Dehaene, I. Denghien, A. Jobert, D. Le Bihan, M. Sigman, C. Pallier, and J.-B. Poline, "Functional segregation of cortical language areas by sentence repetition", *Hum. Brain Mapp.*, vol. 27, pp. 360–371, 2006.

[54] B. Biswal, F. Z. Yetkin, V. M. Haughton, and J. S. Hyde, "Functional connectivity in the motor cortex of resting human brain using echo-planar MRI", *Magn. Reson. Med.*, vol. 34, pp. 537–541, 1995.

[55] G. Tononi, G. Edelman, and O. Sporns, "Complexity and coherency: integrating information in the brain", *Trends in cognitive neuroscience*, vol. 2, pp. 474–484, 1998.

[56] J. S. Damoiseaux, S. A. R. B. Rombouts, F. Barkhof, P. Scheltens, C. J. Stam, S. M. Smith, and C. F. Beckmann, "Consistent resting-state networks across healthy subjects.", *Proc. Natl. Acad. Sci. USA*, vol. 103, pp. 13848–13853, Sep. 2006.

[57] V. El Kouby, Y. Cointepas, C. Poupon, D. Rivière, N. Golestani, J.-B. Poline, D. L. Bihan, and J.-F. Mangin, "Mr diffusion-based inference of a fiber bundle model from a population of subjects", in *MICCAI'05*, 2005, pp. 196–204.

[58] M. D. Fox, A. Z. Snyder, J. M. Zacks, and M. E. Raichle, "Coherent spontaneous activity accounts for trial-to-trial variability in human evoked brain responses.", *Nat Neurosci*, vol. 9, pp. 23–25, Jan. 2006.

[59] M. D. Fox, A. Z. Snyder, J. L. Vincent, and M. E. Raichle, "Intrinsic fluctuations within cortical systems account for intertrial variability in human evoked brain responses", *Proc. Natl. Acad. Sci. USA*, vol. 56, pp. 171–84, Oct. 2007.

[60] D. A. Fair, N. U. F. Dosenbach, J. A. Church, A. L. Cohen, S. Brahmbhatt, F. M. Miezin, D. M. Barch, M. E. Raichle, S. E. Petersen, and B. L. Schlaggar, "Development of distinct control networks through segregation and integration.", *Proc Natl Acad Sci U S A*, vol. 104, pp. 13507–13512, Aug 2007.

[61] D. Cordes, V. M. Haughton, K. Arfanakis, G. J. Wendt, P. A. Turski, C. H. Moritz, M. A. Quigley, and M. E. Meyerand, "Mapping functionally related regions of brain with functional connectivity MR imaging", *Am. J. Neuroradiology*, vol. 21, pp. 1636–1644, Sep. 2000.

[62] P.-J. Lahaye, J.-B. Poline, G. Flandin, S. Dodel, and L. Garnero, "Functional connectivity: studying non-linear, delayed interactions between BOLD signal", *Neuroimage*, vol. 20, pp. 962–974, 2003.

[63] A. Roebroeck, E. Formisano, and R. Goebel, "Mapping directed influence over the brain using granger causality and fmri.", *Neuroimage*, vol. 25, pp. 230–242, Mar 2005.

[64] V. Perlbarg, P. Bellec, J.-L. Anton, M. Pï£¡lï£¡grini-Issac, J. Doyon, and H. Benali, "CORSICA: correction of structured noise in fMRI by automatic identification of ICA components", *Magn. Reson. Imaging*, vol. 25, pp. 35–46, Jan. 2007.

[65] D. Cordes, V. Haughton, J. Carew, K. Arfanakis, and K. Maravilla, "Hierarchical clustering to measure connectivity in fMRI resting-state data.", *Magn. Reson. Imaging*, vol. 20, pp. 305–17, 2002.

[66] M. Voultsidou, S. Dodel, and J. Herrmann, "Neural networks approach to clustering of activity in fMRI data", *IEEE Trans. Med. Imag.*, vol. 24, pp. 987–996, 2005.

Philippe Ciuciu was born in France in 1973. He graduated from the École Supérieure d'Informatique Électronique Automatique, Paris, France, in 1996. He received also the DEA and Ph.D. degrees in signal processing from the Université de Paris-sud, Orsay, France, in 1996 and 2000, respectively.

In November 2000, he joined the fMRI signal processing group as a post-doctoral fellow at Service Hospitalier Frédéric Joliot (CEA, Life Science Division, Medical Research Department) in Orsay, France. Since November 2001, he is a permanent CEA research scientist. In 2007 he moved to NeuroSpin, an ultra high magnetic field Neurospin centre in the LNAO lab. Currently, he am Principal Investigator of the neurodynamics program in collaboration with Andreas Kleinschmidt (DR INSERM) at the Cognitive Neuroimaging Unit (INSERM/CEA U562).

His research is focused on the application of statistical methods (eg, Bayesian inference, model selection), stochastic agorithms (MCMC) and wavelet-based regularized approaches to functional brain imaging (fMRI) and to parallel MRI reconstruction (OPTIMED/ANR project).

Patrice Abry was born in Bourg-en-Bresse, France in 1966. He is Agrégé de Sciences Physiques (1989) and completed a Ph.D. in Physics and Signal Processing in 1994. Since october 95, he is a permanent CNRS researcher, at the Laboratoire de Physique of Ecole Normale Supérieure de Lyon. Patrice Abry received the AFCET-MESR-CNRS prize for best Ph.D. in Signal Processing for the years 93-94 and is the author of a book "Ondelettes et Turbulences", Diderot, 1997. Since 2004, he is member of the SPS-SPTM committee. His current research interests include the wavelet based analysis and modeling of scaling phenomena, of hydrodynamic turbulence and computer network teletraffic.

Cecile Rabrait was born in Montmorency, France in 1980. She is He is Agrégé de Sciences Physiques (2003) and received her M.S. degrees in Physics at the Ecole Normale SupÃl'rieure de Lyon (Lyon, France) in 2004. She completed her Ph.D. degree in Medical Imaging from Neurospin centre (CEA) and Paris-Sud University (Orsay, France) in 2007. She is now working as a Magnetic Resonance Methods Expert for Philips (Best, The Netherlands).

Herwig Wendt was born in Steyr, Austria in 1979. He received the M.S. degree in Electrical Engineering and Telecommunications from Vienna University of Technology, Austria, in 2005. He is currently working toward the Ph.D. degree in Physics and Signal Processing at the Laboratoire de Physique at Ecole Normale Supérieure de Lyon, France. His research interests include scale invariance phenomena, point processes, extreme values, bootstrap methods and machine learning.